

# $\beta$ decay of neutron-rich $^{53-56}\text{Ca}$

P.F. Mantica<sup>(1,2)</sup>, R. Broda<sup>(3)</sup>, H.L. Crawford<sup>(1,2)</sup>, A. Damaske<sup>(1,2)</sup>,  
B. Fornal<sup>(3)</sup>, A.A. Hecht<sup>(4,5)</sup>, C. Hoffman<sup>(6)</sup>, M. Horoi<sup>(7)</sup>, N. Hoteling<sup>(4,5)</sup>,  
R.V.F. Janssens<sup>(5)</sup>, J. Pereira<sup>(1,8)</sup>, J.S. Pinter<sup>(1,2)</sup>, J.B. Stoker<sup>(1,2)</sup>,  
S.L. Tabor<sup>(6)</sup>, T. Sumikama<sup>(9)</sup>,\* W.B. Walters<sup>(6)</sup>, X. Wang<sup>(5,10)</sup>, and S. Zhu<sup>(5)</sup>

<sup>(1)</sup> *National Superconducting Cyclotron Laboratory,*

*Michigan State University, East Lansing, Michigan 48824, USA*

<sup>(2)</sup> *Department of Chemistry, Michigan State University,*

*East Lansing, Michigan 48824, USA*

<sup>(3)</sup> *Institute of Nuclear Physics, Polish Academy of Sciences, PL-31342, Cracow, Poland*

<sup>(4)</sup> *Department of Chemistry and Biochemistry,*

*University of Maryland, College Park, Maryland 20742, USA*

<sup>(5)</sup> *Physics Division, Argonne National Laboratory, Argonne, Illinois 60439, USA*

<sup>(6)</sup> *Department of Physics and Astronomy,*

*Florida State University, Tallahassee, Florida 32306, USA*

<sup>(7)</sup> *Department of Physics, Central Michigan University,*

*Mount Pleasant, Michigan 48859, USA*

<sup>(8)</sup> *Joint Institute for Nuclear Astrophysics,*

*Michigan State University, East Lansing, Michigan 48824, USA*

<sup>(9)</sup> *RIKEN, 2-1 Hirosawa, Wako-shi, Saitama 351-0198, Japan and*

<sup>(10)</sup> *Department of Physics, University of Notre Dame, South Bend, Indiana 46556, USA*

(Dated: November 7, 2018)

## Abstract

$\beta$ -decay properties of neutron-rich Ca isotopes have been obtained. Half-life values were determined for the first time for  $^{54}\text{Ca}$  ( $86 \pm 7$  ms),  $^{55}\text{Ca}$  ( $22 \pm 2$  ms), and  $^{56}\text{Ca}$  ( $11 \pm 2$  ms). The half-life of  $230 \pm 60$  ms deduced for  $^{53}\text{Ca}$  is significantly longer than reported previously, where the decay chain  $^{53}\text{K} \rightarrow ^{53}\text{Ca} \rightarrow ^{53}\text{Sc}$  was considered. A delayed  $\gamma$  ray with energy 247 keV was identified following  $\beta$  decay of  $^{54}\text{Ca}$ , and is proposed to depopulate the  $1_1^+$  level in  $^{54}\text{Sc}$ . The  $\beta$ -decay properties compare favorably with the results of shell model calculations completed in the full  $pf$ -space with the GXPF1 interaction. The half-lives of the neutron-rich Ca isotopes are also compared with gross  $\beta$ -decay theory. The systematic trend of the neutron-rich Ca half-lives is consistent with the presence of a subshell gap at  $N = 32$ .

## INTRODUCTION

The appearance of added stability in atomic nuclei at certain nucleon numbers prompted the development of the nuclear shell model. The robustness of the magic numbers at 2, 8, 20, 28, 50, 82, and 126 has been well demonstrated for nuclei near the valley of  $\beta$  stability. However, only limited data are available for  $\beta$ -unstable nuclei with magic numbers of protons and/or neutrons. In several instances, the observed properties of such radioactive nuclei are not consistent with predictions assuming stabilized proton and/or neutron cores. As examples, the non-existence of  ${}^2_8\text{O}_{20}$  [1], the appearance of an island of inversion around  ${}^{32}\text{Mg}_{20}$  [2, 3] and suspected collectivity at  ${}^{56}_{28}\text{Ni}_{28}$  [4, 5] all call to question a simple extrapolation of the known magic numbers to the drip-lines of the nuclear chart.

The Ca isotopes have a closed-shell number of protons ( $Z = 20$ ) and have been well studied in the range of the doubly-magic nuclei  ${}^{40}\text{Ca}_{20}$  and  ${}^{48}\text{Ca}_{28}$ , where neutrons fill the  $1f_{7/2}$  orbital. Beyond doubly-magic  ${}^{48}\text{Ca}$ , neutrons begin filling the upper  $pf$  shell. Neutron transfer data [6, 7, 8] are available for levels in  ${}^{49}\text{Ca}_{29}$ , and the deduced spectroscopic factors signify energy gaps between the adjacent  $2p_{3/2}$ ,  $2p_{1/2}$ , and  $1f_{5/2}$  single-particle orbitals. Such gaps suggest added stability for the Ca isotopes with  $N = 32$  and  $N = 34$ . Indeed, a subshell closure at  $N = 32$  for  ${}^{52}\text{Ca}$  [9, 10],  ${}^{54}\text{Ti}$  [11], and  ${}^{56}\text{Cr}$  [12] has been inferred from the systematic variation of first-excited  $2^+$  states in the even-even isotopes of these elements as a function of neutron number. The yrast structures of the even-even Cr [13, 14] and Ti [11, 15] isotopes at higher spins also show irregular energy spacings at  $N = 32$  that can be understood if a significant gap in neutron single-particle states between  $\nu p_{3/2}$  and  $\nu p_{1/2}$ ,  $\nu f_{5/2}$  exists. Additional support for the apparent shell gap at  $N = 32$  is found in the small  $B(E2 : 0^+ \rightarrow 2^+)$  values measured for  ${}^{54}\text{Ti}_{32}$  [16] and  ${}^{56}\text{Cr}_{32}$  [17]. No substantial experimental evidence for an expected [18] subshell closure at  $N = 34$  has been found to date, as the even-even Cr [12, 19] and Ti [20] isotopes show a decrease in energy of the  $2^+_1$  level when moving from  $N = 32$  to  $N = 34$ .

Little data are available on the structures of the neutron-rich Ca isotopes beyond  ${}^{52}\text{Ca}_{32}$ . Knowledge of existence has only been extended to  ${}^{56}\text{Ca}_{36}$  [21]. The heaviest Ca isotope where structure and half-life information is available is  ${}^{53}\text{Ca}$ . The  $\beta$ -decay half-life of  ${}^{53}\text{Ca}$  was deduced to be  $90 \pm 15$  ms [22]. In that study,  ${}^{53}\text{Ca}$  was produced from the decay of  ${}^{53}\text{K}$ , which was made directly by fragmentation of an Ir target by light ions, and extracted from an

ion source. The mass-separated sample was studied via  $\beta$ -delayed neutron spectroscopy. A two-component decay curve was observed, and the component with the longer decay constant was attributed to the daughter  $^{53}\text{Ca}$  decay. A delayed neutron branch of  $(40 \pm 10)\%$  was obtained for  $^{53}\text{Ca}$ . A subsequent  $\beta$ -decay study of  $^{53}\text{K}$  [23] revealed a single bound state at 2.2 MeV above the  $^{53}\text{Ca}$  ground state. Significant neutron branching was also observed for the decay of  $^{53}\text{K}$ , but no additional information on the  $\beta$ -decay properties of the  $^{53}\text{Ca}$  daughter was reported in Ref. [23].

We report results of  $\beta$ -delayed  $\gamma$ -ray spectroscopic measurements of  $^{53-56}\text{Ca}$  to examine the robustness of the  $Z = 20$  proton shell closure for very neutron-rich Ca isotopes. The half-lives of  $^{54-56}\text{Ca}$  were determined for the first time, and a longer half-life value was deduced for  $^{53}\text{Ca}$ . The systematic trend in half-life values for the neutron-rich Ca isotopes is compared to predictions from gross  $\beta$  decay and shell model calculations completed in the full  $pf$ -shell model basis.

## EXPERIMENTAL METHODS

Neutron-rich Ca nuclei were produced by fragmentation of a 140 MeV/nucleon  $^{76}\text{Ge}$  beam at National Superconducting Cyclotron Laboratory at Michigan State University. The primary beam was incident on a 352 mg/cm<sup>2</sup> Be target at the object position of the A1900 fragment separator [24]. Two independent settings of the A1900 separator were used to separate the desired isotopes from unwanted reaction products. The first setting was optimized for production of  $^{54}\text{K}$  with magnetic rigidities  $B\rho_1 = 4.4030$  Tm and  $B\rho_2 = 4.1339$  Tm, and included  $^{55,56}\text{Ca}$ . The second A1900 setting with  $B\rho_1 = 4.3867$  Tm and  $B\rho_2 = 4.1339$  Tm was chosen to center the production of  $^{54}\text{Ca}$  at the A1900 focal plane without changing the tune of the second half of the spectrometer (and the downstream beam transport magnets). The particle identification spectra collected at the experimental end station for both A1900 settings are presented in Fig. 1. The full momentum acceptance of the A1900 ( $\sim 5\%$ ) was used for fragment collection. An Al wedge of thickness 300 mg/cm<sup>2</sup> was placed at the intermediate momentum-dispersive image to provide differential energy loss to fragments of differing  $Z$  traversing the spectrometer. A thin plastic scintillator detector was also placed near this position, and position information deduced from this detector was used to correct the fragment time of flight.

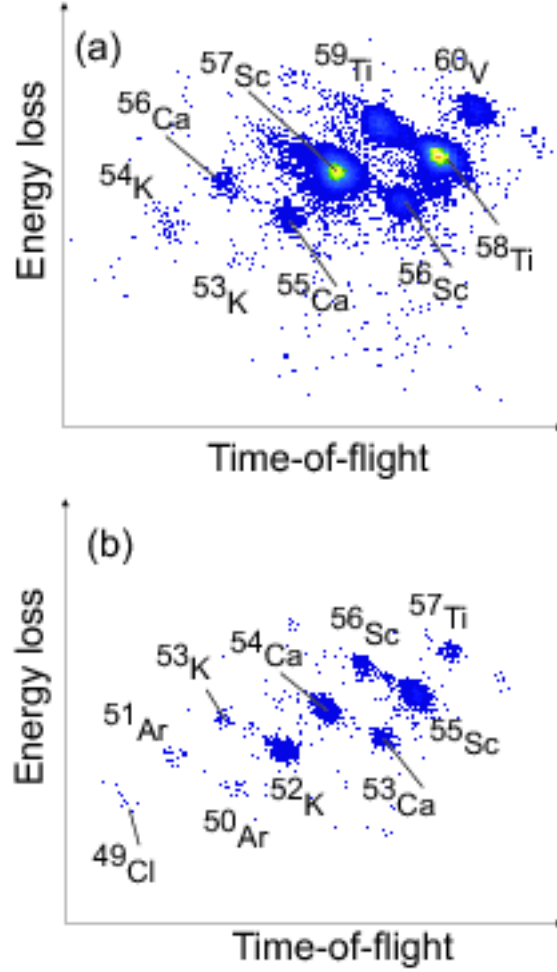


FIG. 1: (Color online) Particle identification spectra for A1900 spectrometer settings where (a)  $^{54}\text{K}$  and (b)  $^{54}\text{Ca}$  were centered in the dispersive plane at the final focus of the device. The energy loss measurement is from the most upstream Si PIN detector of the Beta Counting System with thickness  $991\ \mu\text{m}$ .

The experimental end station consisted of detectors from the Beta Counting System [25] and the Segmented Germanium Array [26]. The fragments transported from the A1900 to the experimental end station first encountered a stack of three Si PIN detectors with thicknesses  $991$ ,  $997$ , and  $309\ \mu\text{m}$ . These detectors provided energy loss information on the incoming beam, critical for particle identification. The timing signal from the most upstream Si PIN was used in conjunction with the cyclotron radiofrequency to deduce fragment time of flight information. The Si PIN stack was followed by a Si double-sided multistrip detector (DSSD) and six Si single-sided multistrip detectors (SSSDs). The DSSD had thickness  $979\ \mu\text{m}$  and was segmented into 40 strips on both front and back, for a total of 1600 pixels. The

SSSDs had nominal thicknesses of 1 mm and were segmented into 16 strips. The SSSDs strip orientation alternated between horizontal and vertical (relative to ground) for each successive detector to provide two-dimensional position information for particles moving downstream of the DSSD. The majority of fragments were stopped in either the DSSD or the most upstream SSSD; a consequence of the large momentum acceptance of the A1900 separator.

Sixteen detectors from the Segmented Germanium Array were arranged in two concentric rings around the vacuum beam line surrounding the Si detectors of the Beta Counting System. The  $\gamma$ -ray peak detection efficiency was 20% at 100 keV and 7% at 1 MeV. The energy resolution of each Ge detector in the array was  $\sim 3.5$  keV for the 1.3 MeV  $\gamma$ -ray transition in  $^{60}\text{Co}$ .

The master trigger for event readout was determined by a logical OR of any of the following three conditions: 1) signal above threshold in any of the 16 strips of the most upstream SSSD; 2) signal above threshold in any of the 40 front strips AND any of the 40 back strips of the DSSD; 3) signal above threshold in the most upstream Si PIN detector (used for prompt  $\gamma$ -ray detection).  $\gamma$  rays detected within 15  $\mu\text{s}$  of a master trigger were recorded into the event stream. The long gating time for  $\gamma$  rays enabled identification of potential microsecond isomers populated either in the fragmentation process or following  $\beta$  decay. Each event was tagged with an absolute time stamp based on a 50 MHz oscillator that was input to a 32-bit free-running scaler. Details of an implantation event, including energy loss and time-of-flight information required for particle identification, were stored in a two-dimensional array with indices based on pixel location. Correlations with the energy-loss signal from  $\beta$ -decay electrons detected in the DSSD were then processed, based on temporal and position information. Position correlations were restricted to  $\beta$ -decay electrons that emanated from the same pixel or one of the surrounding eight pixels of an implantation. Time correlations had two defined limits: a maximum time for a single  $\beta$ -decay event for a given implantation event and a minimum time for back-to-back implantation events into the same pixel. The details of the implantation event were cleared from the two-dimensional array when these defined limits were not satisfied. The results presented in the next section were obtained with a maximum correlation time of 1 s and a minimum time for back-to-back implantations of 1 s.

## RESULTS

The decay curves for  $^{53-56}\text{Ca}$  are given in Fig. 2. The half-life of each nuclide was deduced by fitting the decay curves to a function that considered exponential decay of the parent, exponential growth and decay of the daughter, and constant background. Decay information on the daughter nuclide was taken from the literature, with additional details provided in the following subsections. Table I summarizes the half-life results for  $^{53-56}\text{Ca}$ .

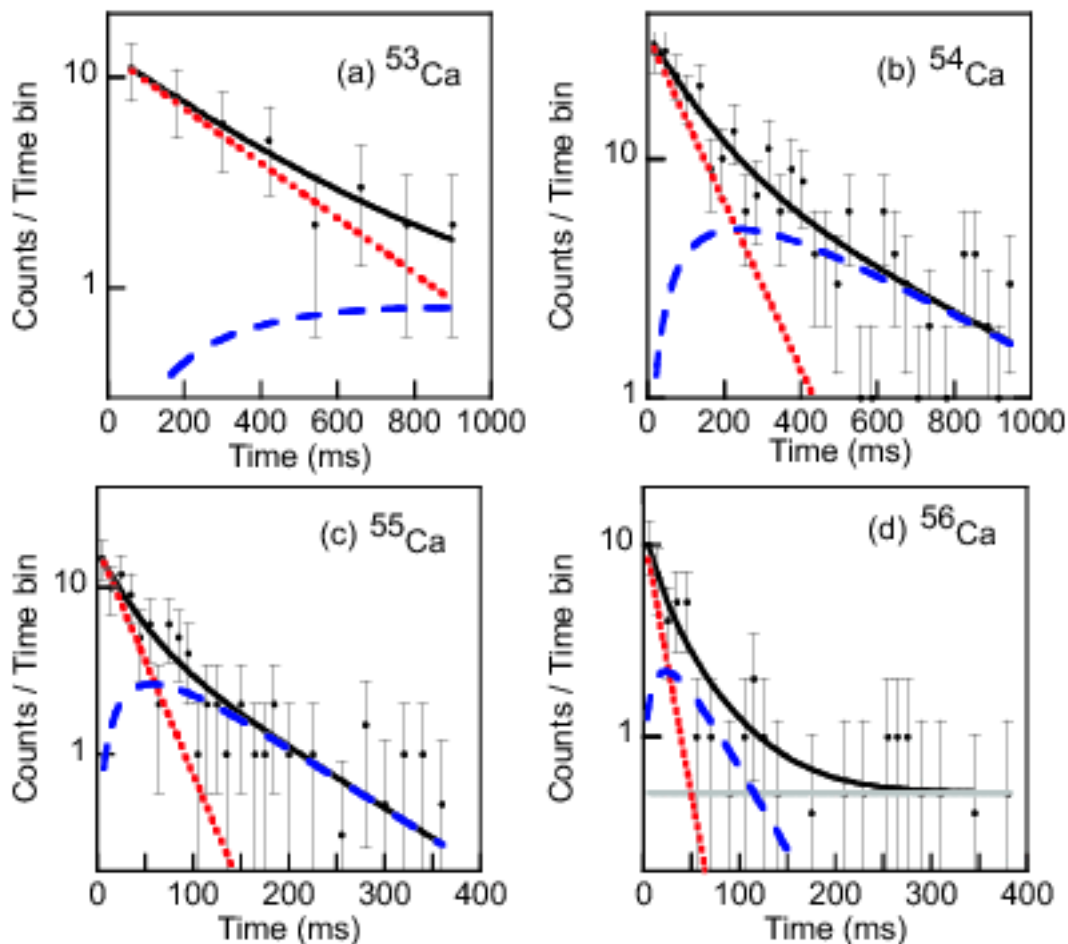


FIG. 2: (Color online) Decay curves for: (a)  $^{53}\text{Ca}$ ; (b)  $^{54}\text{Ca}$ ; (c)  $^{55}\text{Ca}$ ; and (d)  $^{56}\text{Ca}$ . The fitting function (solid black line) considered contributions from parent exponential decay (dotted line), daughter exponential growth and decay (dashed line), and a flat background (solid gray line). The only fitted curve that resulted in a non-negligible value for the background term was that for  $^{56}\text{Ca}$ . Additional details regarding the fitting procedure used to extract half-life values are provided in the text.

TABLE I: Correlation statistics and half-lives deduced for the neutron-rich  $^{53-56}\text{Ca}$  isotopes.

Nuclide	No. Parent Nuclei		$T_{1/2}$ (ms)	
	Implanted	Correlated	This Work	Previous
$^{53}\text{Ca}$	209	32	$230 \pm 60$	$90 \pm 15$ <sup>a</sup>
$^{54}\text{Ca}$	654	136	$86 \pm 7$	
$^{55}\text{Ca}$	246	52	$22 \pm 2$	
$^{56}\text{Ca}$	99	18	$11 \pm 2$	

<sup>a</sup>Ref. [22]

The spectra of  $\gamma$  rays correlated with the  $\beta$  decays of  $^{53-56}\text{Ca}$  are presented in Fig. 3.  $^{54}\text{Ca}$  is the only nuclide where a delayed  $\gamma$  ray is assigned to the parent  $\beta$  decay. No evidence for isomeric  $\gamma$ -ray emission within  $15 \mu\text{s}$  of an implantation was found for the neutron-rich  $^{53-56}\text{Ca}$  isotopes.

More detailed discussions are included below on the results for each isotope.

### $^{53}\text{Ca}$

The half-life of  $^{53}\text{Ca}$  reported here,  $T_{1/2} = 230 \pm 60$  ms, is significantly longer than the value  $90 \pm 15$  ms reported in Ref. [22]. The previous half-life value was deduced following the decay chain  $^{53}\text{K} \rightarrow ^{53}\text{Ca} \rightarrow ^{53}\text{Sc}$ , where  $^{53}\text{K}$  was directly produced by proton spallation of an Ir target and only  $\beta$  particles in coincidence with delayed neutrons were recorded. In that work, data collected in the range 300 to 700 ms were fitted with a single exponential decay, assuming contributions from neither the parent nor the grand-daughter over this time range. These assumptions are reasonable considering the short half-life of  $^{53}\text{K}$ ,  $30 \pm 5$  ms [22], and the unknown, but expected long ( $> 3$  s) half-life of  $^{53}\text{Sc}$  [27]. The decay curve presented in Fig. 2 considers only direct production of  $^{53}\text{Ca}$ , with no ambiguity regarding the fit to a convoluted spectrum involving both parent and daughter decays.

In the present work, the decay curve derived from  $\beta$ -delayed neutron events, presented in Fig. 2 of Ref. [22], was refitted with a function based on the Batemann equations, where the parent exponential decay and daughter exponential growth and decay were considered. The



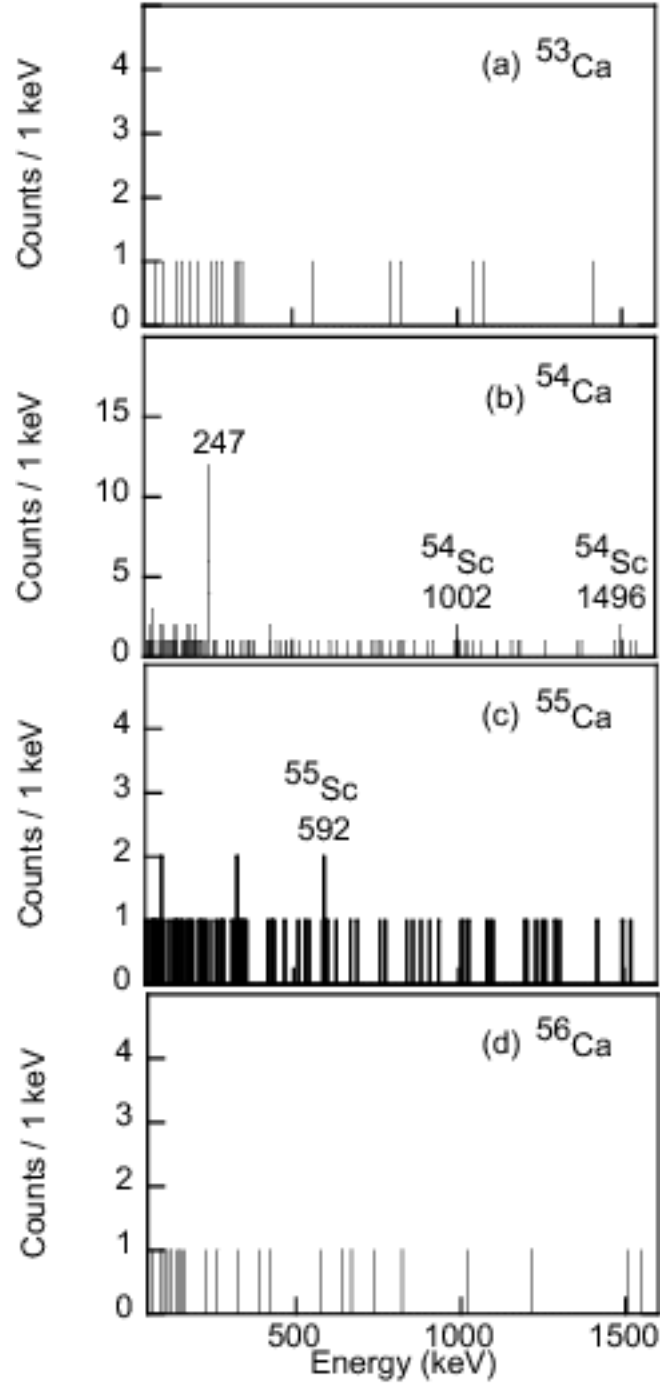


FIG. 3:  $\gamma$ -ray spectrum in the range 50 to 1600 keV correlated with  $\beta$ -decay events for: (a)  $^{53}\text{Ca}$ ; (b)  $^{54}\text{Ca}$ ; (c)  $^{55}\text{Ca}$ ; and (d)  $^{56}\text{Ca}$ . Observed transitions are marked by their energy in keV.

parent half-life value was fixed at 30 ms, and two fixed values of the half-life of the  $^{53}\text{Ca}$  were used: the 90-ms value deduced by Langevin *et al.* [22] and the value of 230 ms deduced here. The parent activity was taken as a free parameter, and the daughter activity was determined as 40% of the parent activity, based on the measured delayed-neutron branching following  $\beta$  decay of this nuclide [22]. The resulting fits are compared with the data in Fig. 4. An  $R^2$  regression analysis to check the goodness of fit produced values of 0.952 and 0.924 for the functions that used  $^{53}\text{Ca}$  half-life values of 90 ms and 230 ms, respectively. The difference in  $R^2$  values between the two fits is not significant, if the errors in the half-life values of the parent (17%) and daughter ( $\sim 20\%$ ) are considered. The longer half-life value deduced here for  $^{53}\text{Ca}$  appears consistent with the  $\beta$ -delayed neutron decay data obtained in the previous study of the  $A = 53$  decay chain.

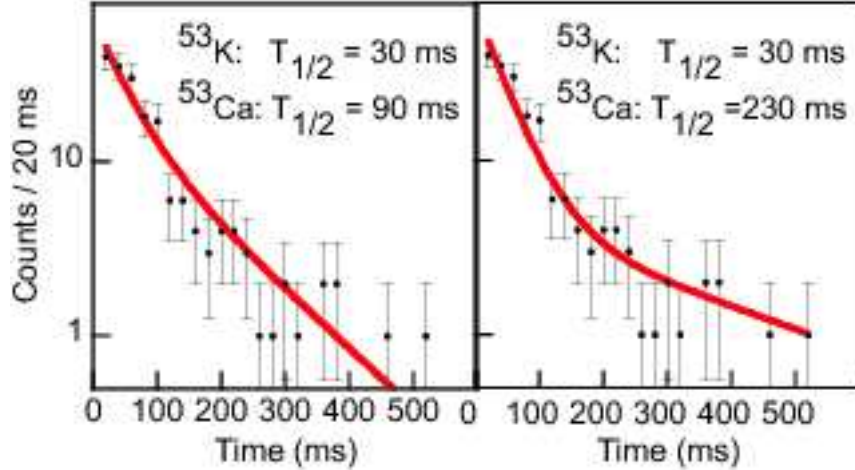


FIG. 4: (Color online)  $\beta$ -delayed neutron decay after collection of  $^{53}\text{K}$  taken from Ref. [22]. Data were fitted with two different half-life values of the daughter  $^{53}\text{Ca}$ . Regression analysis results in  $R^2$  values of 0.952 and 0.924 for the fits with  $^{53}\text{Ca}$  half-life values of 90 ms and 230 ms, respectively.

However, it should be acknowledged that we cannot rule out that the longer half-life measured here could result from the presence of a second  $\beta$ -decaying state in  $^{53}\text{Ca}$ . Isomeric  $J^\pi = 9/2^+$  states are known in the neutron-rich  $^{61}\text{Fe}_{35}$  [28] and  $^{59}\text{Cr}_{35}$  [28, 29] isotopes. Both the magnetic dipole moment [30] and electric quadrupole moment [31] suggest the  $9/2^+$  level in  $^{61}\text{Fe}$  is characterized by a deformed potential. Although the neutron-rich Ti and Ca isotopes should show less deformed structures due to their proximity to the  $Z = 20$  shell closure, the possible influence of the  $\nu g_{9/2}$  orbital on the low-energy structure of these

isotopes requires further investigation.

## $^{54}\text{Ca}$

No previous information on the half-life of  $^{54}\text{Ca}$  was available. The deduced half-life,  $86 \pm 7$  ms, was obtained by fitting the fragment- $\beta$  decay curve in Fig. 2 to a function that included exponential decay of the parent and exponential growth and decay of the  $^{54}\text{Sc}$  daughter (the constant background term was small and could be neglected). The  $^{54}\text{Sc}$  half-life value was fixed at 360 ms [32], while the parent half-life and activity values were free parameters. A single  $\gamma$  ray with energy  $246.9 \pm 0.4$  keV has been assigned to the decay of  $^{54}\text{Ca}$  based on the delayed  $\gamma$ -ray spectrum presented in Fig. 3(b). The decay curve constructed from  $^{54}\text{Ca}$ - $\beta$  correlations with an additional requirement of a coincidence with a 247-keV  $\gamma$  ray is given in Fig. 5. The fitted decay curve returns a half-life consistent with that deduced from the fragment- $\beta$  correlation data.

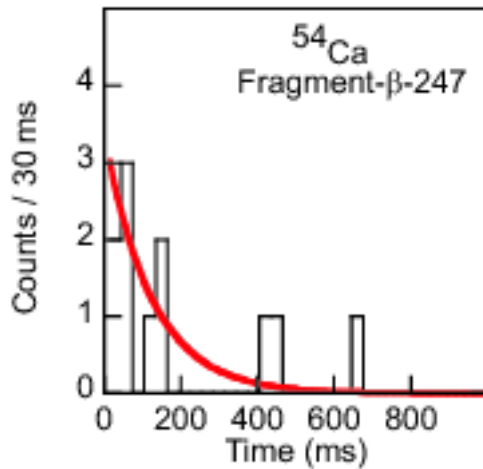


FIG. 5: (Color online) Decay curve for  $^{54}\text{Ca}$  showing fragment- $\beta$  correlations with an additional requirement of a 247-keV  $\gamma$  ray in coincidence. The data were fitted with a single exponential decay with fixed parent half-life (86 ms) and the initial activity as a free parameter.

The absolute intensity of the 247-keV transition was determined to be  $(97 \pm 32)\%$ , based on a Gaussian fit to the  $\gamma$ -ray peak in Fig. 3(b), the measured peak efficiency curve for the 16-detector  $\gamma$ -ray array, and the number of  $^{54}\text{Ca}$  implantations correlated with  $\beta$  decay (see Table I). The absolute intensity implies that a majority of the apparent  $\beta$  intensity from the decay of  $^{54}\text{Ca}$  proceeds through an excited state depopulated by the 247-keV transition. This

transition is proposed to directly feed the ground state of  $^{54}\text{Sc}$ . The new 247-keV excited state is tentatively assigned spin and parity  $1^+$ , based on selection rules for allowed  $\beta$  decay. The uncertainty in the spin and parity assignment for the 247-keV level arises from the large  $Q$  value associated with the  $^{54}\text{Ca}$   $\beta$  decay. The low statistics in the delayed  $\gamma$ -ray spectrum in Fig. 3(b) cannot exclude the presence of higher energy, lower intensity transitions that may directly feed the level at 247 keV. The  $\beta$ -decay sequence and known levels in  $^{54}\text{Sc}$  are displayed in Fig. 6. The decay  $Q$ -value is taken from Ref. [33]. The excited state at 110 keV in  $^{54}\text{Sc}$  was identified as a  $\mu\text{s}$  isomer in studies by Grzywacz *et al.* [28] and was reaffirmed in Ref. [32]. The spin and parity of the  $^{54}\text{Sc}$  ground state was limited to  $(3, 4)^+$ , based on the  $\beta$ -decay feeding pattern to excited states in  $^{54}\text{Ti}$  [11]. Placement of the 247-keV transition would preclude  $J^\pi = 4^+$  for the final state of this “prompt”  $\gamma$ -ray transition, therefore, spin and parity  $3^+$  is proposed for the ground state of  $^{54}\text{Sc}$ . The 247-keV transition is presumed to have  $E2$  multipolarity, and the estimated half-life from Weisskopf estimates of 51 ns is consistent with the “prompt” nature of this transition.

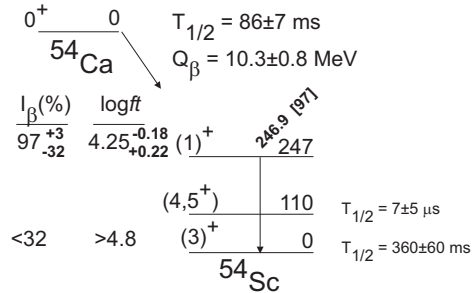


FIG. 6: Low-energy level structure of  $^{54}\text{Sc}$  and  $\beta$ -decay scheme for the parent nuclide,  $^{54}\text{Ca}$ . The energies of each state are given in keV. The level with energy 110 keV was previously identified as a microsecond isomer by Grzywacz *et al.* [28] and later confirmed by Liddick *et al.* [32]. The 110-keV  $\gamma$ -ray was not observed in the  $\beta$ -decay study of  $^{54}\text{Ca}$  presented here.

### $^{55}\text{Ca}$ and $^{56}\text{Ca}$

The only previous information regarding the isotopes  $^{55,56}\text{Ca}$  was their existence, established from fission of relativistic  $^{238}\text{U}$  ions [21]. In that study, six and three counts were associated with the production of  $^{55}\text{Ca}$  and  $^{56}\text{Ca}$ , respectively. We have achieved sufficient statistics in the present study to deduce half-life values for  $^{55,56}\text{Ca}$  for the first time. The

fragment- $\beta$  decay curves were fitted to a function that included the exponential decay of the parent, the growth and decay of the daughter, and a linear background.

For the  $^{55}\text{Ca}$  decay curve in Fig. 2(c), the  $^{55}\text{Sc}$  daughter half-life was fixed to a value  $83 \pm 3$  ms. This new half-life was obtained in the present work from the analysis of  $\beta$ -decay events correlated with  $^{55}\text{Sc}$  implantations shown in Fig. 7, and represents a significant improvement in precision with respect to previously reported values [27, 32]. The parent  $^{55}\text{Ca}$  half-life, initial parent activity, and constant value for background were taken as free parameters. The grand-daughter  $^{55}\text{Ti}$  has a known half-life of  $1.3 \pm 0.1$  s [34] and was not considered in the curve fitting function. The fit resulted in a half-life of  $22 \pm 2$  ms for  $^{55}\text{Ca}$  (see Fig. 2), with a negligible background contribution.

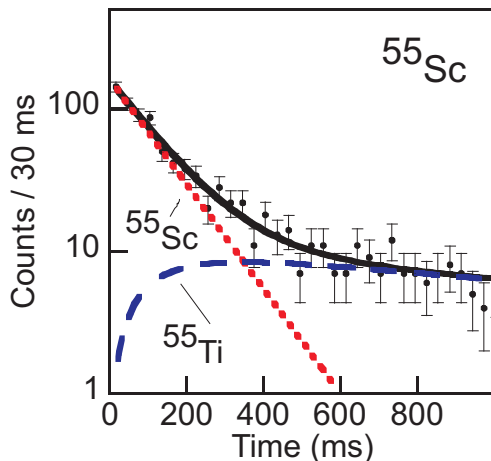


FIG. 7: (Color online) Decay curve for  $\beta$  particles correlated with  $^{55}\text{Sc}$  implantation events. The decay data were fitted to a function (solid black line) that considered the exponential decay of the  $^{55}\text{Sc}$  parent (dotted line) and exponential growth and decay of the  $^{55}\text{Ti}$  daughter (dashed line) with known half-life  $1.3 \pm 0.1$  s [34].

A single  $\gamma$ -ray transition of energy 592 keV was evident in the  $\beta$ -delayed  $\gamma$ -ray spectrum correlated with  $^{55}\text{Ca}$  implantations shown in Fig. 3. This transition was previously assigned to the decay of the  $^{55}\text{Sc}$  daughter [32].

The fit to the  $^{56}\text{Ca}$  decay curve in Fig. 2(d) considered a fixed value of  $35 \pm 5$  ms for the half-life of the  $^{56}\text{Sc}$  daughter. There are, in fact, two  $\beta$ -decaying states in  $^{56}\text{Sc}$  [32]. Decay of the  $^{56}\text{Ca}$  ground state, with presumed spin and parity  $0^+$ , would populate lower-spin states in the daughter nucleus. Therefore, the dominant decay constant to consider for fitting the  $^{56}\text{Ca}$  decay curve is that associated with the low-spin ( $1^+$ ) level in  $^{56}\text{Sc}$ . The half-life

deduced for  $^{56}\text{Ca}$   $\beta$  decay was  $11 \pm 2$  ms, about a factor of two shorter than that in the neighbor  $^{55}\text{Ca}$ . No evidence was found for delayed  $\gamma$ -ray transitions correlated with  $^{56}\text{Ca}$   $\beta$  decays. However, the small number of correlated decays (18 total decay events – see Table I) combined with the measured  $\gamma$ -ray efficiency curve would preclude observation of more than one or two counts for  $\gamma$  rays with energies at the maximum of the Ge array efficiency curve.

## DISCUSSION

### Structure of $^{54}\text{Sc}$

The  $\beta$  decay of  $^{54}\text{Ca}$  apparently proceeds to a single state in  $^{54}\text{Sc}$  residing 247 keV above the ground state. This state has tentatively been assigned  $1^+$  spin and parity. This new information for  $^{54}\text{Sc}$  can be combined with previous knowledge on isomeric and  $\beta$  decay to better understand the coupling of valence protons and neutrons in this odd-odd nucleus.

The known low-energy levels in  $^{54}\text{Sc}$  in Fig. 8 are compared with results of shell model calculations completed in the full  $pf$ -shell model basis with the interactions GXPF1 [18, 35], GXPF1A [36], and KB3G [37]. The difference in calculated level orderings between the GXPF1 and KB3G interactions can be related to the relative energies of the neutron single-particle  $f_{5/2}$  and  $p_{1/2}$  orbitals. The  $3^+$ ,  $4^+$  doublet near the ground state in  $^{54}\text{Sc}$  in the calculations with the GXPF1 and GXPF1A interactions arises from the coupling of the  $\nu p_{1/2}$  and  $\pi f_{7/2}$  orbitals. This configuration appears lowest in energy in  $^{54}\text{Sc}$  since the effective single-particle energy of the  $\nu p_{1/2}$  orbital is below that of the  $\nu f_{5/2}$  orbital with the GXPF1 and GXPF1A interactions. The first  $1^+$  level is attributed mainly to the coupling of the  $\nu f_{5/2}$  and  $\pi f_{7/2}$  single-particle orbitals. This level is at the ground state in the shell-model results with the KB3G interaction, as this interaction places the effective single-particle energy of the  $\nu p_{1/2}$  orbital above that of the  $\nu f_{5/2}$  orbital. The position of the tentative  $1^+$  level at 247 keV assigned in this work, relative to the  $(3)^+$  ground state, is not well reproduced by either the KB3G, GXPF1, or GXPF1A interactions.

The GXPF1 interaction proved successful in reproducing the yrast structures of the Ti isotopes up to  $^{56}\text{Ti}_{34}$ , where the first excited  $2^+$  state was found to have an energy of 1129 keV [20], nearly 400 keV below the GXPF1 expectation. Modification of three two-body

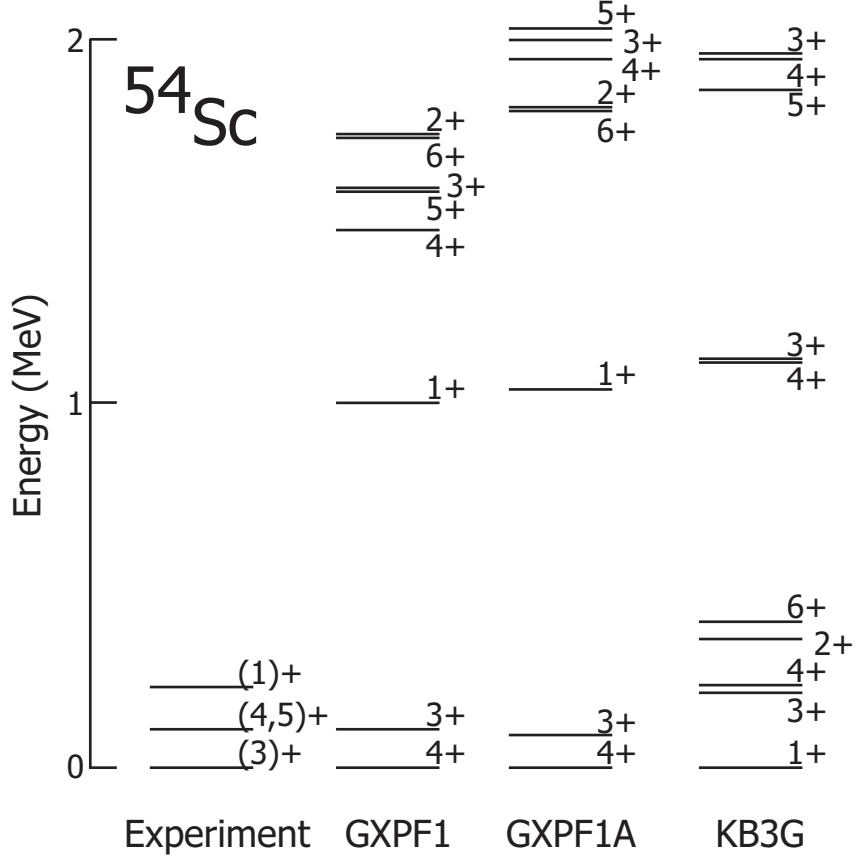


FIG. 8: Low-energy structure of  $^{54}\text{Sc}$  compared to results of shell model calculations employing the GXPF1 [18, 35], GXPF1A [36], and KB3G [37] effective interactions.

pairing matrix elements associated with the  $f_{5/2}$ ,  $f_{7/2}$ , and  $p_{1/2}$  orbitals and two quadrupole-quadrupole interaction matrix elements coupling the  $f_{5/2}$  and  $p_{1/2}$  orbitals to  $J = 2$  and  $J = 3$  resulted in the GXPF1A interaction [36]. The shell model results with the GXPF1A interaction reproduced the low-energy yrast structure of  $^{56}\text{Ti}$  [15] better, while maintaining good agreement with the known level structures of the less neutron-rich Ti isotopes. As noted above, neither interaction does well in reproducing the position of the tentative  $1^+$  state in  $^{54}\text{Sc}$  at 247 keV, which should be dominated by the shell model configuration  $\pi f_{7/2}^1 \nu f_{5/2}^1$ . The low energy of the  $(1)^+$  level relative to the proposed  $(3)^+$  ground state, with dominant configuration  $\pi f_{7/2}^1 \nu f_{5/2}^1$ , suggests that while the level ordering of the  $p_{1/2}$  and  $f_{5/2}$  neutron single-particle orbitals in the GXPF1 and GXPF1A interactions is likely correct, the effective energy spacing between the neutron  $p_{1/2}$  and  $f_{5/2}$  orbitals is overestimated or the interaction strength between  $\pi f_{7/2}^1$  and  $\nu f_{5/2}^1$  is underestimated.

Another outstanding question with regards to the low-energy structure of  $^{54}\text{Sc}$  is the

tentative spin-parity assignment for the isomeric state located 110 keV above the ground state. Grzywacz *et al.* [28] deduced  $E2$  multipolarity for the 110 keV  $\gamma$  ray, based on a comparison of the experimental half-life value  $(7 \pm 5)\mu\text{s}$  with single-particle estimates. Tentative spin and parity  $5^+$  was then assigned to the 110-keV excited state. In Ref. [32], it was suggested that the  $E2$  isomer may represent the decay of the first excited  $1^+$  state, whose energy may be lower than predicted by the shell model calculations utilizing the GXPF1 interaction. Indeed, the  $1_1^+$  state is lower than predicted, tentatively established in  $^{54}\text{Sc}$  at 247 keV. Regardless of the interaction employed, the first excited  $5^+$  state, associated with the  $\pi f_{7/2}^1\nu f_{5/2}^1$  configuration, is expected at an energy in excess of 1.5 MeV (see Fig. 8). The shell model results all suggest a doublet of levels with  $J^\pi = 3^+, 4^+$  near the  $^{54}\text{Sc}$  ground state. These two levels belong to the odd-odd  $\pi f_{7/2}^1\nu p_{1/2}^1$  multiplet. The transition probabilities  $B(M1; 3^+ \rightarrow 4^+)$  and  $B(E2; 3^+ \rightarrow 4^+)$  calculated with the GXPF1 and GXPF1A interactions are listed in Table II, along with the calculated half-lives. The  $M1$  strength dominates, but the calculated partial half-life was in the range of a few nanoseconds, much longer than the 9.3 ps half-life calculated from single-particle estimates. The  $M1$  hindrance factor appears significant for this  $\gamma$ -ray transition. Therefore, the long ( $\mu\text{s}$ ) half-life established for the isomeric transition in  $^{54}\text{Sc}$  does not exclude possible  $4^+$  spin and parity for the first-excited state.

TABLE II: Transition probabilities and partial half-lives for the  $\gamma$ -ray transition between the  $3^+$  and  $4^+$  members of the  $\pi f_{7/2}^1\nu p_{1/2}^1$  multiplet in  $^{54}\text{Sc}$ . The experimental transition energy of 110 keV was used in the calculations.

Multipolarity	GXPF1	GXPF1A	Single-particle
$B(M1; 3^+ \rightarrow 4^+) (\mu^2)$	0.026	0.0037	
$T_{1/2}(M1; 3^+ \rightarrow 4^+) (s)$	$1.1 \times 10^{-9}$	$7.9 \times 10^{-9}$	$9.3 \times 10^{-12}$
$B(E2; 3^+ \rightarrow 4^+) (e^2 fm^4)$	4.50	5.55	
$T_{1/2}(E2; 3^+ \rightarrow 4^+) (s)$	$5.7 \times 10^{-6}$	$4.6 \times 10^{-6}$	$2.9 \times 10^{-6}$

An alternative scenario for the low-energy structure of  $^{54}\text{Sc}$  is that the  $3^+$  and  $4^+$  states of the  $\nu p_{1/2}$   $\pi f_{7/2}$  multiplet are nearly degenerate in energy at the ground state. The close energy spacing between these states would preclude a  $\gamma$ -ray transition between them. The 247-keV transition observed following the  $\beta$  decay of  $^{54}\text{Ca}$  would then be an  $E2$  transition



between the  $1^+$  and  $3^+$  levels, while the isomeric 110-keV  $\gamma$  ray would also have  $E2$  multipolarity and would represent the transition between the  $6^+$  and  $4^+$  levels. Clearly, further studies will be required to provide additional insight into the low-energy structure of  $^{54}\text{Sc}$ .

### $\beta$ decay half-lives of Ca isotopes

#### *Gross Theory*

Gross  $\beta$ -decay theory provides a means for predicting  $\beta$ -decay properties of nuclides far from the valley of stability. The  $\beta$ -decay half-lives are inversely proportional to the Fermi function, and hence, the  $\beta$ -decay  $Q$  value raised to the fifth power:  $T_{1/2} \sim Q_\beta^{-5}$ . In practice, half-life values calculated from gross theory are too long, as the decay strength to low-energy states is underestimated [38]. Tachibana *et al.* [39] extended traditional gross  $\beta$ -decay theory to include a one-particle strength function for the Gamow-Teller decay. Pfeiffer, Kratz, and Möller [40] took a more phenomenological approach to address missing  $\beta$  strength to low-energy states by relating the half-life and  $Q$  value in a manner similar to that employed by Kratz and Herrmann [41] to extract  $P_n$  values:

$$T_{1/2} \sim a \times (Q_\beta - C)^{-b} \quad (1)$$

Here,  $a = 2740$  s and  $b = 4.5$  are taken as constants, and  $C$  is a cutoff energy related to the pairing gap in the daughter nucleus [42]. The results of the two extensions to gross theory for the neutron-rich Ca isotopes are compared with experiment in Fig. 9. The two approaches predict similar half-life values in the range  $^{54-59}\text{Ca}$ . The calculations compare favorably with the experimental half-lives of  $^{53,54}\text{Ca}$ . Both predict too long half-lives for the more neutron-rich  $^{55,56}\text{Ca}$  isotopes, a continuing issue with gross  $\beta$ -decay theory, especially far from the valley of stability, where  $Q_\beta$  is large. The other apparent deficiency in the calculations occurs at  $^{51,52}\text{Ca}$ , as the calculated short half-lives do not consider the known subshell closure at  $N = 32$  for Ca.

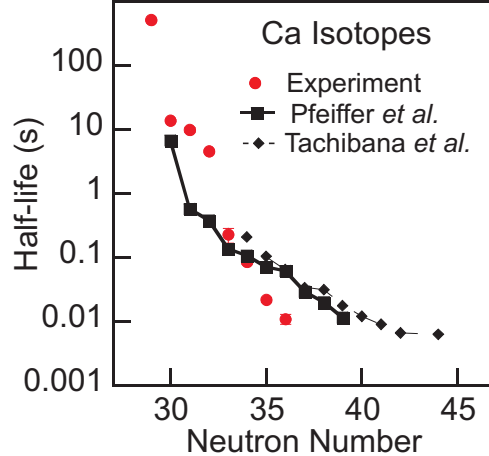


FIG. 9: (Color online) Experimental half-life values of neutron-rich Ca isotopes (filled circles) compared with predictions of gross  $\beta$ -decay theory extended by Tachibana *et al.* [39] and Pfeiffer *et al.* [40].

#### *QRPA results and the fast $\beta$ decays of $^{54-56}\text{Ca}$*

Möller, Nix and Kratz [43] compiled an extensive database of ground-state properties of nuclides across the nuclear chart, including  $\beta$ -decay properties. Nuclear deformations were based on the Finite-Range Droplet Model [44], and Gamow-Teller  $\beta$ -decay rates were calculated in the framework of the quasi-particle Random Phase Approximation (QRPA). The half-lives from the QRPA calculations are compared with experiment for the neutron-rich Ca isotopes in Fig. 10. Möller *et al.* [45] extended the QRPA compilations reported in Ref. [43] to include first-forbidden  $\beta$  decays. Such decays should, in general, be more important for nuclides nearer stability, where  $Q_\beta$  values are small. Comparison of the previously calculated half-lives of the neutron-rich Ca isotopes with this new approach showed little difference, therefore, only the QRPA results for the Gamow-Teller decay rates are given in Fig. 10.

The trend in calculated half-lives follows well the experimental values over the range  $^{50-56}\text{Ca}$ . Again, the slow rate of the  $^{52}\text{Ca}$   $\beta$  decay is indicative of the subshell gap at  $N = 32$ . The strong odd-even effect apparent in the QRPA calculations is not manifested in the experimental half-lives. Indeed, it is only in  $^{52}\text{Ca}$  that a deviation occurs from the regularly decreasing half-lives in the Ca isotopes. That  $^{54}\text{Ca}_{34}$  follows this regular behavior and shows a (relatively) fast  $\beta$  decay may indicate that an appreciable subshell gap at

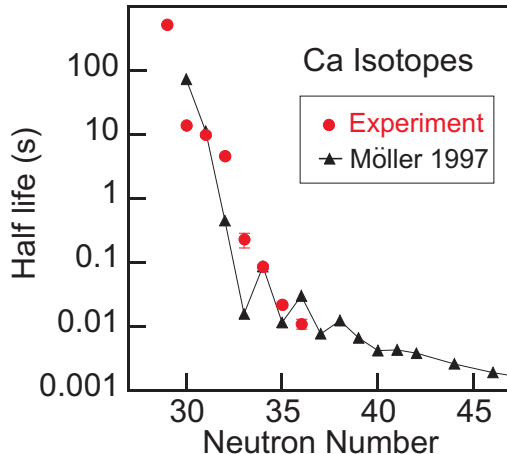


FIG. 10: (Color online) Experimental half-life values of neutron-rich Ca isotopes (filled circles) compared with predictions of the QRPA compilation of Möller *et al.* [43].

$N = 34$  has not developed for the Ca isotopes.

The fast  $\beta$  decays observed experimentally in  $^{55,56}\text{Ca}$  reflect the spin-flip nature of these processes. The last neutron(s) in  $^{55}\text{Ca}_{35}$  and  $^{56}\text{Ca}_{36}$  should occupy the  $f_{5/2}$  neutron orbital.  $\beta^-$  decay is expected to proceed as the spin-flip decay  $\nu f_{5/2} \rightarrow \pi f_{7/2}$ . Such fast decays should have small  $\log ft$  values, and the most prominent  $\beta$ -decay branch should be to the ground state of the daughter. Expectations regarding the  $\beta$ -decay branching in the neutron-rich Ca isotopes are discussed in the next section.

#### *Shell Model results with GXPF1*

The  $\beta$ -decay properties of the  $^{53-56}\text{Ca}$  isotopes were calculated with the shell model effective interaction GXPF1 [18, 35] in the full  $pf$  model space with the CMICHSM [46] code.  $\beta$ -decay  $Q$  values were taken from Ref. [33], and the Gamow-Teller rates were quenched by a factor of 0.77, as explained in Ref. [37]. The calculated half-lives agree within a factor of two with experimental values as demonstrated in Fig. 11. A summary of the shell model results is also given in Table III.

The  $\beta$  decay of  $^{53}\text{Ca}$  from the presumed  $J^\pi = 1/2^-$  ground state is predicted to feed the first excited  $3/2^-$  state in  $^{53}\text{Sc}$  with intensity 60% of the total feeding strength. The  $\beta$  strength to neutron unbound states is calculated to be 6%, which is smaller than that observed in Ref. [22]. The expected decay of  $^{54}\text{Ca}$  is similar to that of  $^{53}\text{Ca}$ . About 60% of

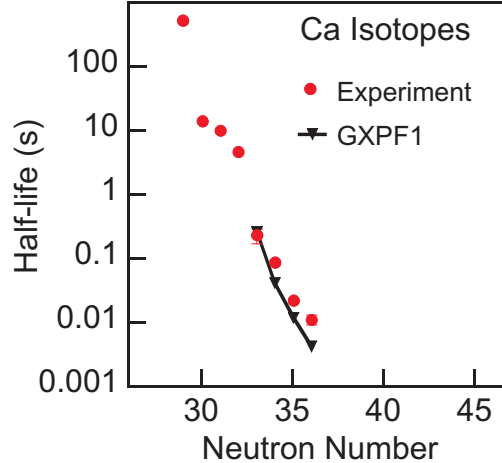


FIG. 11: (Color online) Experimental half-life values of neutron-rich Ca isotopes (filled circles) compared with results of shell model calculations in the full  $pf$ -model space with the GXPF1 interaction.

TABLE III: Shell model results with the effective interaction GXPF1 for the  $\beta$ -decay properties of  $^{54-56}\text{Ca}$ . Experimental values were obtained in this work, unless otherwise indicated.

Nuclide	$J^\pi$	$T_{1/2}^{calc.}$ (ms)	$T_{1/2}^{exp.}$ (ms)	$P_n^{calc.}$ (%)	$P_n^{exp.}$ (%)	calc. g.s. Branch (%)
$^{53}\text{Ca}$	$1/2^-$	264	$230 \pm 60$	6	$40 \pm 10^a$	0
$^{54}\text{Ca}$	$0^+$	41	$86 \pm 7$	6	$< 32$	0
$^{55}\text{Ca}$	$5/2^-$	11.7	$22 \pm 2$	4		92
$^{56}\text{Ca}$	$0^+$	4.3	$11 \pm 2$	2		97

<sup>a</sup>Ref. [22]

the calculated  $\beta$ -decay strength is predicted to feed the first  $1^+$  state in  $^{54}\text{Sc}$ , and the  $P_n$  value is also calculated to be 6%. The observed  $\beta$ -decay strength from  $^{54}\text{Ca}$  is apparently dominated by decay to the the 247-keV level in  $^{54}\text{Sc}$ . The absolute intensity of the 247-keV  $\gamma$ -ray transition that depopulates this state is 97%, with no other peak (intensity threshold  $< 10\%$  below 1 MeV) in the delayed  $\gamma$ -ray spectrum displayed in Fig. 3(b). However, as noted earlier, only tentative  $1^+$  spin and parity have been proposed for this 247-keV level, since the low statistics of the measurement does not rule out the presence of higher-energy  $\gamma$  rays feeding the 247-keV level from potential higher-lying  $1^+$  states. The shell model results with the GXPF1 interaction support the notion that the primary branching in the  $\beta$

decay of  $^{54}\text{Ca}$  is to the first excited  $1^+$  in  $^{54}\text{Sc}$ . The experimental delayed-neutron branching reported in Table III for  $^{54}\text{Ca}$  is governed by the lower limit of the absolute intensity of the 247-keV  $\gamma$  ray.

The  $\beta$ -decay properties of  $^{55,56}\text{Ca}$  were found to be similar to the shell model results, as was the case with  $^{53,54}\text{Ca}$ . The decays are dominated by fast ground state to ground state transitions, which carry more than 90% of the  $\beta$ -decay strength. Since only a small number of decays were detected for both  $^{55}\text{Ca}$  and  $^{56}\text{Ca}$ , there was little possibility to observe branching to excited states in the  $^{55}\text{Sc}$  and  $^{56}\text{Sc}$  daughters, respectively, that would lead to  $\gamma$ -ray or neutron emission. The short half-life values and large, direct ground-state  $\beta$  branching again reflect the dominance of the spin-flip  $\nu f_{5/2} \rightarrow \pi f_{7/2}$  decay process in the shell model results. The good agreement between the experimental and shell model half-lives for  $^{55,56}\text{Ca}$  support the notion that the  $\nu f_{5/2}$  orbital is near the Fermi surface for these nuclides with  $N > 34$ .

## SUMMARY

The  $\beta$ -decay properties of the neutron-rich Ca isotopes have been extended to  $^{56}\text{Ca}_{36}$ . The half-lives of  $^{54-56}\text{Ca}$  have been measured for the first time to be  $86 \pm 7$  ms,  $22 \pm 2$  ms, and  $11 \pm 2$  ms, respectively. A new half-life of  $230 \pm 60$  ms has been deduced for  $^{53}\text{Ca}$ , a value longer than that reported previously. The trend of the  $\beta$ -decay half-lives of the neutron-rich Ca isotopes shows a regular decrease except at  $^{52}\text{Ca}_{32}$ , which is attributed to the known subshell closure at  $N = 32$ . The low-energy structure of  $^{54}\text{Sc}$ , the  $\beta$ -decay daughter of  $^{54}\text{Ca}$ , has been elucidated further. The ground and first excited states most likely arise from coupling of the  $\pi f_{7/2}$  and  $\nu p_{1/2}$  orbitals, suggesting that the  $\nu p_{1/2}$  single-particle orbital resides below the  $\nu f_{5/2}$  state at  $N = 33$ . Such level ordering was also inferred from the low-energy structure of the  $N = 33$  isotone  $^{55}\text{Ti}$  [47]. The first  $1^+$  level in  $^{54}\text{Sc}$  has been proposed at an energy of 247 keV above the ground state. This tentative  $1^+$  level is presumed to be a member of the  $\pi f_{7/2} - \nu f_{5/2}$  multiplet, and is nearly 800 keV lower than shell model predictions with the GXPF1 and GXPF1A effective interactions. It seems that the effective energy gap between adjacent neutron single-particle orbitals  $f_{5/2}$  and  $p_{1/2}$  is overestimated or the interaction strength between the  $\pi f_{7/2}$  and  $\nu f_{5/2}$  orbitals is underestimated by the GXPF1 interaction. The fast  $\beta$  decays of  $^{55,56}\text{Ca}$  agree within a factor of two with the shell model results, where the  $\beta$  strength is dominated by the  $\nu f_{5/2} \rightarrow \pi f_{7/2}$  spin-flip decay. The

shell model prediction for the half-life of  $^{54}\text{Ca}$  is also within a factor of two of experiment. Such good agreement may initially invoke support for a shell closure at  $N = 34$ , since the GXPF1 interaction includes a significant energy gap between adjacent single-particle orbitals  $\nu f_{5/2}$  and  $\nu p_{1/2}$ . However, the  $^{54}\text{Ca}$  half-life is also found to agree well with the predictions of gross  $\beta$  decay theory and the results of QRPA calculations, which do not formally consider a strong shell gap at  $N = 34$ . Therefore, any interpretation regarding magicity at  $^{54}\text{Ca}_{34}$  will require further experimental investigation. Exploring the  $\beta$ -decay properties of heavier Ca isotopes towards  $^{60}\text{Ca}$  will prove challenging due to low production cross sections. However, such studies are vital to better understand the evolution of neutron single-particle states with an increase in isospin and corresponding decrease in neutron separation energy.

The authors thank the NSCL operations staff for providing the primary and secondary beams for this experiment and members of the NSCL Gamma group for assistance in setting up and maintaining the Ge detectors. The work was supported in part by the National Science Foundation grants PHY-06-06007 (NSCL), PHY-02-44453 (JINA), PHY-04-56463 (FSU), and PHY-05-55366 (CMU/MSU) and the U.S. Department of Energy, Office of Nuclear Physics, under contracts DE-AC02-06CH11357 (ANL) and DE-FG02-94-ER40834 (Maryland). Travel support was also provided by the Polish Science Committee grant P03B 059 29.

---

\* Present address: Department of Physics, Tokyo University of Science, 2641 Yamazaki, Noda, Chiba 278-8510, Japan.

- [1] O. Tarasov, R. Allatt, J.C. Angelique, R. Anne, C. Borcea, Z. Dlouhy, C. Donzaud, S. Grevy, D. Guillemaud-Mueller, M. Lewitowicz, S. Lukyanov, A.C. Mueller, F. Nowacki, Yu. Oganessian, N.A. Orr, A.N. Ostrowski, R.D. Page, Yu. Penionzhkevich, F. Pougheon, A. Reed, M.G. Saint-Laurent, W. Schwab, E. Sokol, O. Sorlin, W. Trinder, and J.S. Winfield, *Phys. Lett.* **409B**, 64 (1997).
- [2] E.K. Warburton, J.A. Becker, and B.A. Brown, *Phys. Rev. C* **12**, 644 (1975).
- [3] T. Motobayashi, Y. Ikeda, Y. Ando, K. Ieki, M. Inoue, N. Iwasa, T. Kikuchi, M. Kurokawa, S. Moriya, S. Ogawa, H. Murakami, S. Shimoura, Y. Yanagisawa, T. Nakamura, Y. Watanabe, M. Ishihara, T. Teranishi, H. Okuno, and R.F. Casten, *Phys. Lett. B* **346**, 9 (1995).

- [4] K.L. Yurkewicz, D. Bazin, B.A. Brown, C.M. Campbell, J.A. Church, D.C. Dinca, A. Gade, T. Glasmacher, M. Honma, T. Mizusaki, W.F. Mueller, H. Olliver, T. Otsuka, L.A. Riley, and J.R. Terry, *Phys. Rev. C* **70**, 054319 (2004).
- [5] K. Minamisono, P.F. Mantica, T.J. Mertzimekis, A.D. Davies, M. Hass, J. Pereira, J.S. Pinter, W.F. Rogers, J.B. Stoker, B.E. Tomlin and R.R. Weerasiri, *Phys. Rev. Lett.* **96**, 102501 (2006).
- [6] T.R. Canada, C. Ellegaard, and P.D. Barnes, *Phys. Rev. C* **4**, 471 (1971).
- [7] N. Taccetti, P.A. Mando, P. Sona, and K.P. Lieb, *J. Phys. G* **13**, 393 (1978).
- [8] Y. Uozumi, O. Iwamota, S. Widodo, A. Nohtomi, T. Sakae, M. Matoba, M. Nakano, T. Maki, and N. Koori, *Nucl. Phys.* **A576**, 123 (1994).
- [9] A. Huck, G. Klotz, A. Knipper, C. Mieke, C. Richard-Serre, G. Walter, A. Poves, H.L. Ravn, and G. Marguier, *Phys. Rev. C* **31**, 2226 (1985).
- [10] A. Gade, R.V.F. Janssens, D. Bazin, R. Broda, B.A. Brown, C.M. Campbell, M.P. Carpenter, J.M. Cook, A.N. Deacon, D.-C. Dinca, B. Fornal, S.J. Freeman, T. Glasmacher, P.G. Hansen, B.P. Kay, P.F. Mantica, W.F. Mueller, J.R. Terry, J.A. Tostevin, S. Zhu, *Phys. Rev. C* **74**, 021302 (2006).
- [11] R.V.F. Janssens, B. Fornal, P.F. Mantica, B.A. Brown, R. Broda, P. Bhattacharyya, M.P. Carpenter, M. Cinausero, P.J. Daly, A.D. Davies, T. Glasmacher, Z.W. Grabowski, D.E. Groh, M. Honma, F.G. Kondev, W. Krolas, T. Lauritsen, S.N. Liddick, S. Lunardi, N. Marginean, T. Mizusaki, D.J. Morrissey, A.C. Morton, W.F. Mueller, T. Otsuka, T. Pawlat, D. Seweryniak, H. Schatz, A. Stolz, S.L. Tabor, C.A. Ur, G. Viesti, I. Wiedenhoever, and J. Wrzesinski, *Phys. Lett. B* **546**, 55 (2002).
- [12] J.I. Prisciandaro, P.F. Mantica, B.A. Brown, D.W. Anthony, M.W. Cooper, A. Garcia, D.E. Groh, A. Komives, W. Kumarasiri, P.A. Lofy, A.M. Oros-Peusquens, S.L. Tabor, and M. Wiedeking, *Phys. Lett. B* **510**, 17 (2001).
- [13] D.E. Appelbe, C.J. Barton, M.H. Muikku, J. Simpson, D.D. Warner, C.W. Beausang, M.A. Caprio, J.R. Cooper, J.R. Novak, N.V. Zamfir, R.A.E. Austin, J.A. Cameron, C. Malcolmson, J.C. Waddington, and F.R. Xu, *Phys. Rev. C* **67**, 034309 (2003).
- [14] S. Zhu, A.N. Deacon, S.J. Freeman, R.V.F. Janssens, B. Fornal, M. Honma, F.R. Xu, R. Broda, I.R. Calderin, M.P. Carpenter, P. Chowdhury, F.G. Kondev, W. Krolas, T. Lauritsen, S.N. Liddick, C.J. Lister, P.F. Mantica, T. Pawlat, D. Seweryniak, J.F. Smith, S.L. Tabor, B.E. Tomlin, B.J. Varley, and J. Wrzesinski, *Phys. Rev. C* **74**, 064315 (2006).

- [15] B. Fornal, S. Zhu, R.V.F. Janssens, M. Honma, R. Broda, P.F. Mantica, B.A. Brown, M.P. Carpenter, P.J. Daly, S.J. Freeman, Z.W. Grabowski, N.J. Hammond, F.G. Kondev, W. Krolas, T. Lauritsen, S.N. Liddick, C.J. Lister, E.F. Moore, T. Otsuka, T. Pawlat, D. Seweryniak, B.E. Tomlin, and J. Wrzesinski, *Phys. Rev. C* **70**, 064304 (2004).
- [16] D.-C. Dinca, R.V.F. Janssens, A. Gade, D. Bazin, R. Broda, B.A. Brown, C.M. Campbell, M.P. Carpenter, P. Chowdhury, J.M. Cook, A.N. Deacon, B. Fornal, S.J. Freeman, T. Glasmacher, M. Honma, F.G. Kondev, J.-L. Lecouey, S.N. Liddick, P.F. Mantica, W.F. Mueller, H. Olliver, T. Otsuka, J.R. Terry, B.A. Tomlin and K. Yoneda, *Phys. Rev. C* **71**, 041302 (2005)
- [17] A. Bürger, T.R. Saito, H. Grawe, H. Hübel, P. Reiter, J. Gerl, M. Górska, H.J. Wollersheim, A. Al-Khatib, A. Banu, T. Beck, F. Becker, P. Bednarczyk, G. Benzoni, A. Bracco, S. Brambilla, P. Bringel, F. Camera, E. Clément, P. Doornenbal, H. Geissel, A. Görngen, J. Grebosz, G. Hammond, M. Hellström, M. Honma, M. Kavatsyuk, O. Kavatsyuk, M. Kmiecik, I. Kojouharov, W. Korten, N. Kurz, R. Lozeva, A. Maj, S. Mandal, B. Million, S. Muralithar, A. Neusser, F. Nowacki, T. Otsuka, Zs. Podolyák, N. Saito, A.K. Singh, H. Weick, C. Wheldon, O. Wieland, M. Winkler, and RISING Collaboration, *Phys. Lett. B* **622**, 29 (2005).
- [18] M. Honma, T. Otsuka, B.A. Brown, and T. Mizusaki, *Phys. Rev. C* **65**, 061301 (2002).
- [19] O. Sorlin, C. Donzaud, F. Nowacki, J.C. Angelique, F. Azaiez, C. Bourgeois, V. Chiste, Z. Dlouhy, S. Grevy, D. Guillemaud-Mueller, F. Ibrahim, K.-L. Kratz, M. Lewitowicz, S.M. Lukyanov, J. Mrazek, Yu.-E. Penionzhkevich, F. de Oliveira Santos, B. Pfeiffer, F. Pougheon, A. Poves, M.G. Saint-Laurent and M. Stanoiu, *Eur. Phys. J. A* **16**, 55 (2003).
- [20] S.N. Liddick, P.F. Mantica, R.V.F. Janssens, R. Broda, B.A. Brown, M.P. Carpenter, B. Fornal, M. Honma, T. Mizusaki, A.C. Morton, W.F. Mueller, T. Otsuka, J. Pavan, A. Stolz, S.L. Tabor, B.E. Tomlin, and M. Wiedeking, *Phys. Rev. Lett.* **92**, 072502 (2004).
- [21] M. Bernas, C. Engelmann, P. Armbruster, S. Czajkowski, F. Ameil, C. Bockstiegel, Ph. Dessagne, C. Donzaud, H. Geissel, A. Heinz, Z. Janas, C. Kozhuharov, Ch. Mische, G. Munzenberg, M. Pfutzner, W. Schwab, C. Stephan, K. Summerer, L. Tassan-Got, and B. Voss, *Phys. Lett.* **415B**, 111 (1997).
- [22] M. Langevin, C. Detraz, D. Guillemaud-Mueller, A.C. Mueller, C. Thibault, F. Touchard, G. Klotz, C. Mische, G. Walter, M. Epherre, and C. Richard-Serre, *Phys. Lett. B* **130**, 251 (1983).



- [23] F. Perrot, F. Marechal, C. Jollet, Ph. Dessagne, J.-C. Angelique, G. Ban, P. Baumann, F. Benrachi, U. Bergmann, C. Borcea, A. Buta, J. Cederkall, S. Courtin, J.-M. Daugas, L.M. Fraile, S. Grevy, A. Jokinen, F.R. Lecolley, E. Lienard, G. Le Scornet, V. Meot, Ch. Mieke, F. Negroita, N.A. Orr, S. Pietri, E. Poirier, M. Ramdhane, O. Roig, I. Stefan, and W. Wang, *Phys.Rev. C* **74**, 014313 (2006).
- [24] D.J. Morrissey, B.M. Sherrill, M. Steiner, A. Stolz, and I. Wiedenhöver, *Nucl. Instrum. Methods Phys. Res. B* **204**, 90 (2003).
- [25] J.I. Prisciandaro, A.C. Morton, and P.F. Mantica, *Nucl. Instrum. Methods Phys. Res. A* **505**, 140 (2003).
- [26] W.F. Mueller, J.A. Church, T. Glasmacher, D. Gutknecht, G. Hackman, P.G. Hansen, Z. Hu, K.L. Miller, P. Quirin, *Nucl. Instrum. Methods Phys. Res. A* **466**, 492 (2001).
- [27] O. Sorlin, V. Borrel, S. Grevy, D. Guillemaud-Mueller, A.C. Mueller, F. Pougheon, W. Bohmer, K.-L. Kratz, T. Mehren, P. Möller, B. Pfeiffer, T. Rauscher, M.G. Saint-Laurent, R. Anne, M. Lewitowicz, A. Ostrowski, T. Dörfler, and W.-D. Schmidt-Ott, *Nucl. Phys.* **A632**, 205 (1998).
- [28] R. Grzywacz, R. Beraud, C. Borcea, A. Emsallem, M. Glogowski, H. Grawe, D. Guillemaud-Mueller, M. Hjorth-Jensen, M. Houry, M. Lewitowicz, A.C. Mueller, A. Nowak, A. Plochocki, M. Pfützner, K. Rykaczewski, M.G. Saint-Laurent, J.E. Sauvestre, M. Schaefer, O. Sorlin, J. Szerypo, W. Trinder, S. Viteritti, and J. Winfield, *Phys. Rev. Lett.* **81**, 766 (1998).
- [29] S.J. Freeman, R.V.F. Janssens, B.A. Brown, M.P. Carpenter, S.M. Fischer, N.J. Hammond, M. Honma, T. Lauritsen, C.J. Lister, T.L. Khoo, G. Mukherjee, D. Seweryniak, J.F. Smith, B.J. Varley, M. Whitehead, and S. Zhu, *Phys. Rev. C* **69**, 064301 (2004).
- [30] I. Matea, G. Georgiev, J.M. Daugas, M. Hass, G. Neyens, R. Astabatyanyan, L.T. Baby, D.L. Balabanski, G. Belier, D. Borremans, G. Goldring, H. Goutte, P. Himpe, M. Lewitowicz, S. Lukyanov, V. Meot, F. de Oliveira Santos, Yu.E. Penionzhkevich, O. Roig, and M. Sawicka, *Phys. Rev. Lett.* **93**, 142503 (2004).
- [31] N. Vermeulen, S.K. Chamoli, J.M. Daugas, M. Hass, D.L. Balabanski, J.P. Delaroche, F. de Oliveira-Santos, G. Georgiev, M. Girod, G. Goldring, H. Goutte, S. Grevy, I. Matea, P. Morel, B.S. Nara Singh, Yu.-E. Penionzhkevich, L. Perrot, O. Perru, S. Peru, O. Roig, F. Sarazin, G.S. Simpson, Yu. Sobolev, I. Stefan, C. Stodel, D.T. Yordanov, and G. Neyens, *Phys. Rev. C* **75**, 051302 (2007).

- [32] S.N. Liddick, P.F. Mantica, R. Broda, B.A. Brown, M.P. Carpenter, A.D. Davies, B. Fornal, T. Glasmacher, D.E. Groh, M. Honma, M. Horoi, R.V.F. Janssens, T. Mizusaki, D.J. Morrissey, A.C. Morton, W.F. Mueller, T. Otsuka, J. Pavan, H. Schatz, A. Stolz, S.L. Tabor, B.E. Tomlin, and M. Wiedeking, *Phys. Rev. C* **70**, 064303 (2004).
- [33] G. Audi, A.H. Wapstra, C. Thibault, J. Blachot, and O. Bersillon, *Nucl. Phys.* **A729**, 1 (2003).
- [34] P.F. Mantica, B.A. Brown, A.D. Davies, T. Glasmacher, D.E. Groh, M. Horoi, S.N. Liddick, D.J. Morrissey, A.C. Morton, W.F. Mueller, H. Schatz, A. Stolz and S.L. Tabor, *Phys. Rev. C* **68**, 044311 (2003).
- [35] M. Honma, T. Otsuka, B.A. Brown, and T. Mizusaki, *Phys. Rev. C* **69**, 034335 (2004).
- [36] M. Honma, T. Otsuka, B.A. Brown, and T. Mizusaki, *Eur. Phys. J. A* **25**, Supplement 1, 499 (2005).
- [37] A. Poves, J. Sanchez-Solano, E. Caurier, and F. Nowacki, *Nucl. Phys.* **A694**, 157 (2001).
- [38] B. Pfeiffer, K.-L. Kratz, and P. Möller, *Prog. Nucl. Energy* **41**, 39 (2002).
- [39] T. Tachibana, M. Yamada, and Y. Yoshida, *Prog. Theor. Phys.* **84**, 641 (1990).
- [40] B. Pfeiffer, K.-L. Kratz, and P. Möller, “Predictions of  $T_{1/2}$  and  $P_n$  Values”, Inst. für Kernchemie, Univ. Mainz Internal Report, 2000.
- [41] K.-L. Kratz and G. Herrmann, *Z. Phys.* **263**, 435 (1973).
- [42] D.G. Madland and J.R. Nix, *Nucl. Phys. bf A476*, 1 (1988).
- [43] P. Möller, J.R. Nix, and K.-L. Kratz, *At. Data Nucl. Data Tables* **66**, 131 (1997).
- [44] P. Möller, J.R. Nix, W.D. Myers, and W.J. Swiatecki, *At. Data Nucl. Data Tables* **59**, 185 (1995).
- [45] P. Möller, B. Pfeiffer, and K.L. Kratz, *Phys. Rev. C* **67**, 055802 (2003).
- [46] M. Horoi, B.A. Brown, and V. Zelevinsky, *Phys. Rev. C* **67**, 034303 (2003).
- [47] S. Zhu, R.V.F. Janssens, B. Fornal, S.J. Freeman, M. Honma, R. Broda, M.P. Carpenter, A.N. Deacon, B.P. Kay, F.G. Kondev, W. Krolas, J. Kozemczak, A. Larabee, T. Lauritsen, S.N. Liddick, C.J. Lister, P.F. Mantica, T. Otsuka, T. Pawlat, A. Robinson, D. Seweryniak, J.F. Smith, D. Steppenbeck, B.E. Tomlin, J. Wrzesinski, and X. Wang *Phys. Lett. B* **650**, 135 (2007)